

Neuronal Excitability

Coordinated Expression of Two Types of Low-Threshold K^+ Channels Establishes Unique Single Spiking of Mauthner Cells among Segmentally Homologous Neurons in the Zebrafish Hindbrain

ID Takaki Watanabe, Takashi Shimazaki, and ID Yoichi Oda

DOI: <http://dx.doi.org/10.1523/ENEURO.0249-17.2017>

Division of Biological Science, Graduate School of Science, Nagoya University, Nagoya, 464-8602, Japan

Abstract

Expression of different ion channels permits homologously-generated neurons to acquire different types of excitability and thus code various kinds of input information. Mauthner (M) series neurons in the teleost hindbrain consist of M cells and their morphological homologs, which are repeated in adjacent segments and share auditory inputs. When excited, M cells generate a single spike at the onset of abrupt stimuli, while their homologs encode input intensity with firing frequency. Our previous study in zebrafish showed that immature M cells burst phasically at 2 d postfertilization (dpf) and acquire single spiking at 4 dpf by specific expression of auxiliary $Kv\beta 2$ subunits in M cells in association with common expression of $Kv1.1$ channels in the M series. Here, we further reveal the ionic mechanisms underlying this functional differentiation. Pharmacological blocking of $Kv7/KCNQ$ in addition to $Kv1$ altered mature M cells to fire tonically, similar to the homologs. In contrast, blocking either channel alone caused M cells to burst phasically. M cells at 2 dpf fired tonically after blocking $Kv7$. *In situ* hybridization revealed specific $Kv7.4/KCNQ4$ expression in M cells at 2 dpf. $Kv7.4$ and $Kv1.1$ channels expressed in *Xenopus* oocytes exhibited low-threshold outward currents with slow and fast rise times, while coexpression of $Kv\beta 2$ accelerated and increased $Kv1.1$ currents, respectively. Computational models, modified from a mouse cochlear neuron model, demonstrated that $Kv7.4$ channels suppress repetitive firing to produce spike-frequency adaptation, while $Kv\beta 2$ -associated $Kv1.1$ channels increase firing threshold and decrease the onset latency of spiking. Altogether, coordinated expression of these low-threshold K^+ channels with $Kv\beta 2$ functionally differentiates M cells among homologous neurons.

Key words: $Kv1.1$; $Kv7.4$; $Kv\beta 2$; Mauthner cell; phasic firing; simulation

Significance Statement

Sensory information is often processed in neural populations with different levels of excitability that extract distinct features of stimuli. It is known that mutations in the low-threshold K^+ channels, $Kv7.4$ and $Kv1.1$, lead to deafness or ataxia in humans, respectively, and losing either channel results in sensory processing impairments due to disrupted phasic excitability in mice. However, how these channels differentially contribute to phasic excitability in a sensory system remains unclear. Here, we show that $Kv7.4$ and $Kv1.1$ channels with $Kv\beta 2$ subunits have distinct roles in phasic-firing in zebrafish hindbrain neurons. Coordinated expression of these channels is developmentally regulated to ensure that among segmentally homologous, tonically bursting neurons, specific neurons acquire single spiking.

Introduction

Neurons exhibit varied intrinsic excitability, as represented by temporal firing patterns in response to step

depolarization. These are basically classified as either phasic- or tonic-firing patterns by the respective presence or absence of spike-frequency adaptation (Carr and

Received July 15, 2017; accepted September 29, 2017; First published October 4, 2017.

The authors declare no competing financial interests.

Author contributions: T.W. and Y.O. designed research; T.W. and T.S. performed research; T.W. contributed unpublished reagents/analytic tools; T.W. analyzed data; T.W. and Y.O. wrote the paper.

Soares, 2002; Prescott and De Koninck, 2002; Maravall et al., 2004; Kalluri et al., 2010). Heterogeneity in firing threshold, duration, onset latency, and spike-frequency adaptation are also observed among phasic-firing neurons, even in specific neural populations (Locke and Nerbonne, 1997; Prescott and De Koninck, 2002; Soares et al., 2002; Reid et al., 2004). Although intrinsic firing properties are acquired developmentally from immature firing to the phasic or tonic type (Nakamura and Takahashi, 2007; Iwasaki et al., 2008; Hoffpauir et al., 2010; Marrs and Spirou, 2012), the underlying molecular mechanisms remain unclear.

Zebrafish and goldfish Mauthner (M) cells, a pair of giant reticulospinal neurons (RSNs) located in the fourth segment of the hindbrain, are known as a vertebrate model that generates only a single action potential (AP) at the onset of noxious sensory input, thereby triggering fast escape behavior (Zottoli, 1977; Nakayama and Oda, 2004; Kohashi and Oda, 2008). In contrast, two paired RSNs that are repeated in adjacent hindbrain segments (MiD2cm and MiD3cm) are morphologically homologous to M cells, and fire tonically with regular spiking at frequencies dependent on input intensity (Nakayama and Oda, 2004). Because M cells and M-cell homologs, collectively called the “M series” (Lee and Eaton, 1991), share direct projections from auditory afferents (Nakayama and Oda, 2004; Szabo et al., 2007), they are thought to play a role in initiating escape by encoding the onset and intensity of sound, respectively (Oertel, 1999). Because the M series is thought to be evolutionarily duplicated (Metcalf et al., 1986), we hypothesized that functional differentiation of intrinsic excitability arises from segmental duplication of a common ancestral neuron accompanied by subsequent variation. Our previous zebrafish study indicated that single spiking of M cells is developmentally acquired at 4 d postfertilization (dpf) from immature phasic-firing by enhancing surface expression of voltage-gated K⁺ (Kv) channel α -subunits, *Kv1.1a/kcna1a* (also known as zKv1.1a), via later developmental expression of auxiliary Kv β 2 subunits *Kv β 2b/kcnab2b* (also known as zKv β 2b; Watanabe et al., 2014). However, the phasic-firing pattern of 4-dpf M cells after pharmacologically blocking Kv1.1 channels substantially differs from repetitive firing at 2 dpf. These results raise the

possibility that other ion channels contribute developmentally to distinct phasic-firing properties specific to M cells among the M series.

Here, we sought to determine the ionic basis for developmentally-acquired differentiation of firing properties among this neural population. We focused on low-threshold K⁺ channels, including the Kv1 and Kv7/KCNQ families (Johnston et al., 2010), which are activated around the resting membrane potential and play a role in generating phasic-firing in sympathetic, auditory, and vestibular mammalian neurons (Brew and Forsythe, 1995; Wang and McKinnon, 1995; Kalluri et al., 2010). Although they have a similar low-threshold activation voltage, Kv7/KCNQ channels exhibit slow activation-kinetics (Wang et al., 1998), whereas Kv1 channels show rapid activation (Hopkins et al., 1994). However, the differential contributions of these channels to phasic firing remains poorly understood.

In this study, we performed *in vivo* whole-cell recordings from M-series neurons in zebrafish embryos and larvae, and examined the effects of pharmacological manipulations of low-threshold K⁺ channels on firing patterns. We first demonstrate that Kv7/KCNQ is responsible for producing phasic behavior in M cells from 2 dpf, which is distinct from the later contribution of Kv1.1. Second, expression analysis of Kv7 α -subunits, electrophysiological assessment of *Xenopus* oocytes, and computational modeling revealed that early expression of Kv7.4/KCNQ4 in M cells mediates slowly-activating currents to produce phasic bursting. Third, later expression of Kv β 2 enhances inhibition of repetitive firing by Kv1.1, resulting in single spiking. Together, the contributions of two different low-threshold Kv channels with an auxiliary subunit differentiate unique M-cell phasic-firing properties from a common tonic-firing property conserved among the M series.

Materials and Methods

Animals

Zebrafish (*Danio rerio*) wild-type and transgenic strains, *Tol-026* (RRID:ZFIN_ZDB-GENO-120508-16) and *Tol-056* (RRID:ZFIN_ZDB-GENO-120316-108), expressing green fluorescent protein (GFP) in M cells and the M-cell homologs MiD2cm and MiD3cm (Kohashi et al., 2012; Watanabe et al., 2014) were reared and staged using established standard protocol. All procedures were performed in compliance with the guidelines approved by the Animal Care and Use Committee of Nagoya University (approval numbers 14-5 and 15-4).

In vivo whole-cell recording

Tol-026 or *Tol-056* strain embryos and larvae at 56–64 h postfertilization (hpf; 2 dpf) and 102–181 hpf (4–7 dpf) were processed as described previously (Watanabe et al., 2014). In brief, to allow access to M cells or M-cell homologs, embryos or larvae were anesthetized with 0.02% tricaine mesylate (MS-222, Sigma-Aldrich), immobilized with 1 mM D-tubocurarine (Sigma-Aldrich), and then pinned and operated on in a silicon dish filled with extra-

This work was supported by Grants-in-Aid for Scientific Research (KAKENHI 22300126, 23650164, 23115508, 25250002) and a fellowship from the Japan Society for the Promotion of Science (KAKENHI 09J09220).

T. Watanabe's present address: Department of Neurophysiology, Graduate School of Medicine, the University of Tokyo, Tokyo 113-0033, Japan

Acknowledgements: We thank Dr. K. Ohsumi of Nagoya University for providing *Xenopus* oocytes and Ms. Y. Matsutani for fish care.

Correspondence should be addressed to either of the following: Takaki Watanabe, Department of Neurophysiology, Graduate School of Medicine, The University of Tokyo, Tokyo 113-0033, Japan, E-mail: wtakaki@m.u-tokyo.ac.jp; or Yoichi Oda, Division of Biological Science, Graduate School of Science, Nagoya University, Furo, Chikusa, Nagoya 464-8602, Japan, E-mail: oda@bio.nagoya-u.ac.jp.

DOI: <http://dx.doi.org/10.1523/ENEURO.0249-17.2017>

Copyright © 2017 Watanabe et al.

This is an open-access article distributed under the terms of the Creative Commons Attribution 4.0 International license, which permits unrestricted use, distribution and reproduction in any medium provided that the original work is properly attributed.

cellular solution containing: 134 mM NaCl, 2.9 mM KCl, 1.2 mM MgCl₂, 2.1 mM CaCl₂, 10 mM HEPES, and 10 mM glucose, adjusted to pH 7.8 with NaOH. Whole-cell recordings from M cells and their homologs were obtained using a MultiClamp 700B amplifier (Molecular Devices) and digitizer (Digidata 1440A; Molecular Devices) at a sampling rate of 50 kHz. Patch-clamp electrodes for whole-cell recordings were pulled from borosilicate glass (GD-1.5; Narishige) and filled with intracellular solution containing: 119 mM K-gluconate, 6 mM KCl, 2 mM MgCl₂, 10 mM HEPES, 10 mM EGTA, and 4 mM Na₂ATP (at 290 mOsm and pH 7.2), and 0.005% Alexa Fluor 594 hydrazide (Life Technologies). Electrode resistance ranged from 3–8 MΩ. During current-clamp recordings, 6,7-dinitroquinoxaline-2,3-dione (DNQX; Tocris Bioscience) and strychnine (Sigma-Aldrich) were added to the extracellular solution at a final concentration of 50 and 5 μM, respectively. For pharmacological experiments, 10,10-bis(4-pyridinylmethyl)-9(10H)-anthracenone (XE991; Tocris Bioscience) and dendrotoxin-I (DTX; Peptide Institute) were added to the bath at a final concentration of 10 μM and 100 nM, respectively. Data were acquired 20 min after adding the pharmacological solutions, and cells with resting membrane potentials lower than –70 mV were analyzed using Clampfit 10 software (Molecular Devices, RRID:SCR_011323). The liquid junction potential (15 mV) was calculated and corrected for data from M cells or their homologs.

Cloning of Kv7/KCNQ channels

Zebrafish Kv7/KCNQ channels comprising Kv7.1/KCNQ1, Kv7.2/KCNQ2, Kv7.3/KCNQ3, Kv7.4/KCNQ4, and Kv7.5/KCNQ5 were identified by a blast search of a zebrafish genomic database (Zv9) using protein sequences from their mammalian counterparts. The N and C termini of a single *Kv7.4/kcnq4* gene were separately located in adjacent genomic regions of zebrafish ENSDARG00000089490 and ENSDARG00000089559, respectively. We performed a polymerase chain reaction following reverse transcription (RT-PCR) with total RNA extracted from embryos (2 dpf) using the following primers: *Kv7.1a/kcnq1a*, 5'-GCTCGAGAGTATTCCTCATTGTGCTTTCCTGC, 5'-GTAGCCAATAGTGGTTACTGTTACC; *Kv7.1b/kcnq1b*, 5'-GCTCGAGGTGCTTCTGTATCACTTCTCCTC, 5'-CTGCCGATGGATAAAAAACCACTG; *Kv7.2a/kcnq2a*, 5'-GCTCGAGATGGTGAAGAAATCCGCCAACG, 5'-GAGAAACCTCAGACTCCTTATGG; *Kv7.2b/kcnq2b*, 5'-GCTCGAGATCACTCTGACCACCATCGG, 5'-GCACTTTAGATGGACTGTCTTCAATG; *Kv7.3/kcnq3*, 5'-GCTCGAGGTTTTGGGATGTCTGATTCTGTCTG, 5'-CGTCTGCATAGGTGTCAAAGTC; *Kv7.4/kcnq4*, 5'-GCTCGAGATGCTGGGTAGTCCTTCCAATAAC, 5'-GGAATTCTCACTCCATGTTACCGCTGTC; *Kv7.5a/kcnq5a*, 5'-GCTCGAGAGTCACGCACAACGACTGAAG, 5'-GAACGAGACACTCCACTACC; *Kv7.5b/kcnq5b*, 5'-GCTCGAGGAAGGTGAGGCTAACGTTACTG, 5'-GGAGTTGTTCTGGTTGAGGTTTC. Truncated or full-length cDNA segments were cloned in a pCR4Blunt-TOPO vector (Life Technologies). After sequencing, full-length amino acid sequences from Zv9 were aligned across vertebrates using

GENETYX software (GENETYX), enabling the construction of phylogenetic trees (Clustal W method).

In situ hybridization

We performed whole-mount and on-section *in situ* hybridization using wild-type embryos (2 dpf) and larvae (5 dpf) with immunostaining and retrograde labeling of RSNs, respectively, as described previously (Watanabe et al., 2014). Briefly, digoxigenin (DIG)-labeled antisense RNA probes, using Kv7 genes as targets and Kv1.1a and Kvβ2b as positive controls, were synthesized *in vitro* using truncated or full-length cDNA, followed by alkaline hydrolysis at 70°C for 10 min to generate 0.5–1.0 kb probes. At 2 dpf, pigmentation-prevented embryos (obtained after 24 hpf by 0.003% 1-phenyl-2-thiourea (PTU) incubation for 24–30 h; Karlsson et al., 2001) were anesthetized with 0.02% MS-222 until immobilized and then fixed at 48–54 hpf in 4% (w/v) paraformaldehyde (PFA) in PBS. Fixed embryos were treated sequentially with 25%, 50%, 75%, and 100% methanol/PBS 0.1% Tween 20 for 5 min each time, and stored with 100% methanol for over 2 h at –20°C. After proteinase K treatment (10 μg/ml; Roche) for 40–60 min, embryos were refixed and hybridized with RNA probes at 65°C for 12–16 h. After washing at 65°C, embryos were incubated with horseradish peroxidase-conjugated anti-DIG antibody (1:2000; Roche) and monoclonal 3A10 antibody [1:50; Developmental Studies Hybridoma Bank (DSHB), RRID:AB_531874] for 12–16 h at 4°C. RNA probes were detected using a tyramide signal amplification (Cardin et al., 2009) kit with Alexa Fluor 488 (Life Technologies) and an anti-mouse IgG secondary antibody conjugated with Alexa Fluor 568 (1:2000; Roche). After removing the yolk, dorsal images of whole-mounted embryos were obtained by confocal microscopy (FV300; Olympus). For 5 dpf, wild-type larvae were injected with 10% (w/v) Alexa Fluor 568 fixable dextran 10,000 MW (Life Technologies) into the caudal spinal cord at 4 dpf, and then fixed in 4% PFA/PBS at 120–125 hpf. After methanol treatment, larvae were incubated in 30% sucrose and embedded in Tissue-Tek O.C.T. compound (Sakura). Thick horizontal sections of larvae (20-μm) were obtained using a cryostat (CM1850; Leica), and treated with proteinase K (5 μg/ml) for 15 min, followed by refixation for 20 min. Sections were then processed using the same protocol as for whole-mount *in situ* hybridization.

Two-electrode voltage-clamp recordings in *Xenopus* oocytes

Xenopus laevis oocytes were collected and treated as previously described (Watanabe et al., 2014), and injected using a Drummond microinjector with 46 nl cRNA (250 ng/μl) synthesized from full-length zebrafish *Kv7.4/kcnq4*, *Kv1.1a/kcna1a*, and *Kvβ2b/kcnab2b* cDNA using a mMESSAGE mMACHINE Kit (Life Technologies). The volume ratio of *Kv1.1a* and *Kvβ2b* cRNA solution was 1:5. K⁺ currents were recorded using two electrodes with a resistance of 0.5–1.0 MΩ (when filled with 3 M KCl), and an Axoclamp 2B amplifier (Molecular Devices). During recordings, oocytes were perfused in a chamber with a bath solution containing: 96 mM NaMeSO₄, 2 mM KCl, 1 mM

MgCl₂, 1 mM CaCl₂, and 5 mM HEPES, adjusted to pH 7.6 with NaOH. Niflumic acid (0.3 mM) was added to block endogenous chloride currents (Hopkins et al., 1994). Transient capacitance and linear leakage currents were subtracted using a P/4 procedure. The conductance-voltage plots were fitted by a standard Boltzmann equation ($G = G_{\max}/[1 + \exp(V_{1/2} - V)/k]$, where $V_{1/2}$ is the voltage of half-maximal activation, and k is the slope factor). Data were analyzed and fitted using Clampfit 10 software (Molecular Devices).

Computational model

We simulated low-threshold K⁺ currents and M cell firing in a single-compartment model of a *Xenopus* oocyte and M cell, respectively, using NEURON simulator (version 7.3, RRID:SCR_005393; Hines and Carnevale, 2001). Our model channel generator and firing simulator are publicly available on Model DB repository (<https://senselab.med.yale.edu/ModelDB>; accession # 232813) and as Extended Data 1. The simulations were based on a Hodgkin-Huxley (H-H) model of a mammalian ventral cochlear nucleus neuron, which like an M cell, possesses a single-spiking property (Rothman and Manis, 2003b). We constructed single cylindrical compartments for the *Xenopus* oocyte model (20- μ m length and 20- μ m diameter) and M-cell model (40- μ m length and 40- μ m diameter), possessing 12 pF and 50 pF, respectively (specific membrane capacitance: $c_m = 1 \mu\text{F}/\text{cm}^2$). These compartments enabled us to directly observe the effects of ion conductances on the cell without cable properties derived from an axon and dendrites or non-uniform localization of ion channels. The parameters of the H-H model for low-threshold K⁺ conductance of each zebrafish Kv7.4 ($g_{\text{Kv7.4}}$), Kv1.1 ($g_{\text{Kv1.1}}$), and Kv1.1 with Kv β 2 ($g_{\text{Kv1.1+Kv}\beta 2}$) were fitted to the data from the *Xenopus* oocyte system described above, by simulating voltage-clamp recordings at a virtual 20°C. The model M cell included the following maximal conductances: 6000 ns, voltage-gated Na⁺ conductance (\bar{g}_{Nav} : 120 ms/cm²); 1500 ns, high-threshold K⁺ conductance (\bar{g}_{high} : 30 ms/cm²); 300 ns, A-type K⁺ conductance (\bar{g}_A : 6 ms/cm²); and 12 ns, leak conductance (\bar{g}_{leak} : 0.24 ms/cm²) and arbitrary low-threshold K⁺ conductance ($\bar{g}_{\text{Kv7.4}}$, $\bar{g}_{\text{Kv1.1}}$, $\bar{g}_{\text{Kv1.1+Kv}\beta 2}$). Additionally, H-H models of g_{Nav} , g_{high} , and g_A were modified from the study by Rothman and Manis (Rothman and Manis, 2003b) to fit M-cell firing and AP wave form. The reversal potentials of Na⁺, K⁺, and the leakage conductances were set to +30 mV, −90 mV, and −85 mV, respectively, and the resting potential of the M-cell model was set to a default of −85 mV, as observed *in vivo* (Watanabe et al., 2014). Current-clamp simulation was conducted at a virtual temperature of 25°C, and the threshold current (1T) was found by 1 pA increments via current injection. The combination effects of Kv7.4 and Kv1.1 for 2-dpf M cells, or Kv7.4 and Kv1.1 with Kv β 2 for 4-dpf M cells were simulated by implementation of ($\bar{g}_{\text{Kv7.4}}$ and $\bar{g}_{\text{Kv1.1}}$) or ($\bar{g}_{\text{Kv7.4}}$ and $\bar{g}_{\text{Kv1.1+Kv}\beta 2}$). Overall, 1071 firing patterns (21 × 51 combinations) were produced by increments of 100 ns for $\bar{g}_{\text{Kv7.4}}$ and 20 ns for $\bar{g}_{\text{Kv1.1}}$ or $\bar{g}_{\text{Kv1.1+Kv}\beta 2}$, ranging from 0 to 2000 ns (40 ms/cm²) and from 0 to 1000 ns (20 ms/cm²), respectively.

Firing properties were analyzed using MATLAB R2013a software (MathWorks, RRID:SCR_001622).

Statistical analysis

The pharmacological experiments in the M cells were analyzed using Mann–Whitney *U* tests for two independent data sets. Two-way repeated measures ANOVA was used for interspike interval (ISI) comparisons because ISI was repeatedly measured from the same cell at different time points from ISI_{1st} to ISI_{12th}. We used the Kruskal–Wallis test with the *post hoc* Bonferroni-corrected Mann–Whitney *U* test for analysis of the *Xenopus* oocyte system. Statistical analysis was conducted in EZR (Kanda, 2013). All data are represented as mean ± SEM.

Results

Coordinated contribution of Kv7/KCNQ and Kv1 channels to single spiking in zebrafish M cells

To identify the ion channels responsible for establishing the unique single-spiking property of M cells among M-series neurons, we first examined the effect of pharmacologically blocking low-threshold K⁺ channels on firing patterns in response to step depolarization. *In vivo* whole-cell recordings from zebrafish M cells at 4–7 dpf revealed typical single spiking at the onset of step depolarization, which contrasts the tonic firing of the M-cell homologs repeated in adjacent segments (i.e., MiD2cm and MiD3cm; Fig. 1). Bathing with either DTX or XE991, specific blockers for Kv1 or Kv7 channels, respectively, caused M cells to burst phasically (Fig. 1A). After treatment with both DTX and XE991, M cells showed tonic firing or regular spiking at frequencies that depended on the injected current intensity, similar to the segmental homologs (Fig. 1A,B; Nakayama and Oda, 2004; Watanabe et al., 2014). We quantitatively illustrated the effect of K⁺ channel blockers by plotting the number of spikes elicited by depolarizing current pulses against the current intensity (Fig. 1C). We found no significant difference in the ISI compared with M-cell homologs (Fig. 1D). These results demonstrate that both DTX- and XE991-sensitive Kv1 and Kv7, respectively, are responsible for acquisition of the single-spiking property by M cells. Hence, coordinated expression of both types of low-threshold K⁺ channels is likely a key step for functional differentiation of M cells as possessing a single-spiking activity pattern that distinguishes them from their homologous neurons.

It should be noted that DTX- and XE991-sensitive K⁺ channels may contribute differentially to M-cell excitability, because DTX treatment decreased threshold current intensity for spiking, and prolonged the time to spike initiation (spike latency) from stimulus onset at threshold intensity, whereas XE991 treatment alone did not affect these properties (Fig. 1E,F). Moreover, there was a tendency for a more prolonged spike latency with both DTX and XE991 treatment (Fig. 1F; see Discussion).

Kv7/KCNQ channels are required for phasic bursting of immature M cells

Since immature M cells are known to burst (Fig. 2; Watanabe et al., 2014), we next examined the contribution

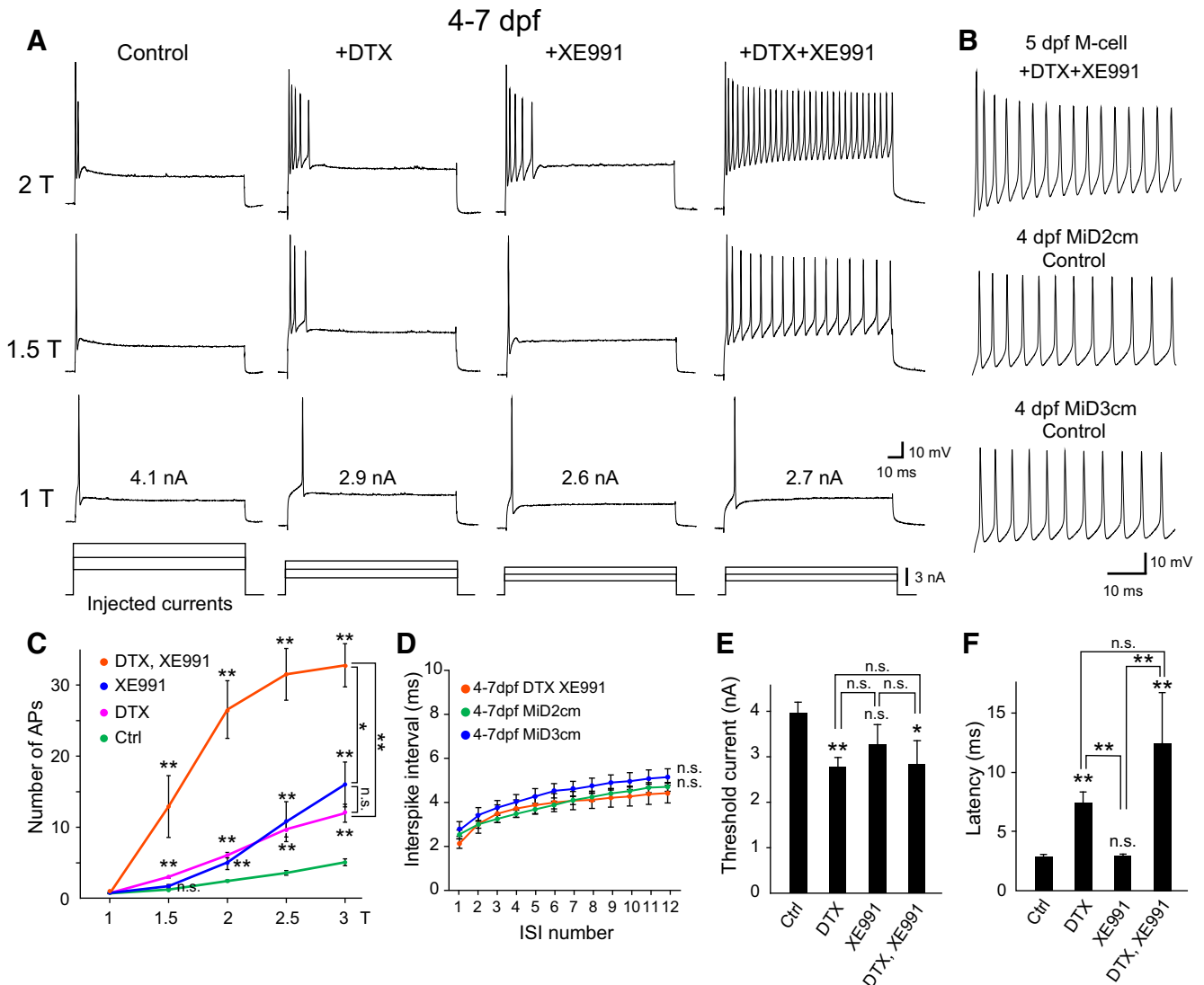


Figure 1. Effect of DTX and/or XE991 on single spiking in developed M cells. **A**, Firing response of M cells at 4–7 dpf [upper three rows of traces elicited by step depolarizing currents (lower traces) of 1×, 1.5×, and 2× threshold intensity (T), as represented in nA on 1T traces] before and after bath application of either 100 nM DTX, 10 μM XE991, or both. **B**, Initial phase of repetitive firing in response to 2T current injection recorded from M cells with DTX and XE991 treatment, and untreated (control) MiD2cm and MiD3cm cells at 4 dpf. **C**, Number of APs elicited during a depolarizing current pulse (100 ms) plotted against current intensity (T). The number of APs significantly increased after combined DTX and XE991 treatment compared with each separately. **D**, Summary data for the ISI of repetitive firing in response to 2T current injection against the interval number. After combined DTX and XE991 treatment, M cells at 4–7 dpf exhibited ISIs that were similar to untreated MiD2cm and MiD3cm cells at the same developmental stage. **E**, **F**, The effect of DTX and/or XE991 on threshold current (**E**) and onset latency of the first spike at 1T (**F**). Treatment of DTX, but not XE991, reduced the threshold current and increased spiking latency of M cells. n.s., not significant. * $p < 0.05$, ** $p < 0.01$, Mann–Whitney U test (control, $n = 14$; +DTX, $n = 8$; +XE991, $n = 7$; +DTX + XE991, $n = 6$). Two-way repeated measures ANOVA was used for ISI (MiD2cm, $n = 8$; MiD3cm, $n = 7$).

of both types of low-threshold K^+ channels on M-cell firing during early development. Blocking $Kv1$ channels with DTX treatment had little effect on immature zebrafish M cells at 2 dpf (Fig. 2A), as we previously reported (Watanabe et al., 2014). In contrast, blocking $Kv7$ channels with XE991 treatment significantly enhanced excitability, especially at the later phase of step depolarization, resulting in tonic firing at regular intervals (Fig. 2A). This quality was also exhibited by M-cell homologs in control preparations. We summarized the effects by plotting

spike number against depolarizing current intensity (Fig. 2B). Immature M cells exhibited spike adaptation with increasing ISI at the later phase, with adaptation completely abolished by XE991 (Fig. 2A,C). XE991 treatment also affected the spike latency of M cells (Fig. 2E). These results indicate that XE991-sensitive K^+ channels mainly contribute to phasic bursting of M cells at the early stage of development. However, some contribution of DTX-sensitive channels cannot be excluded because threshold current and spike latency

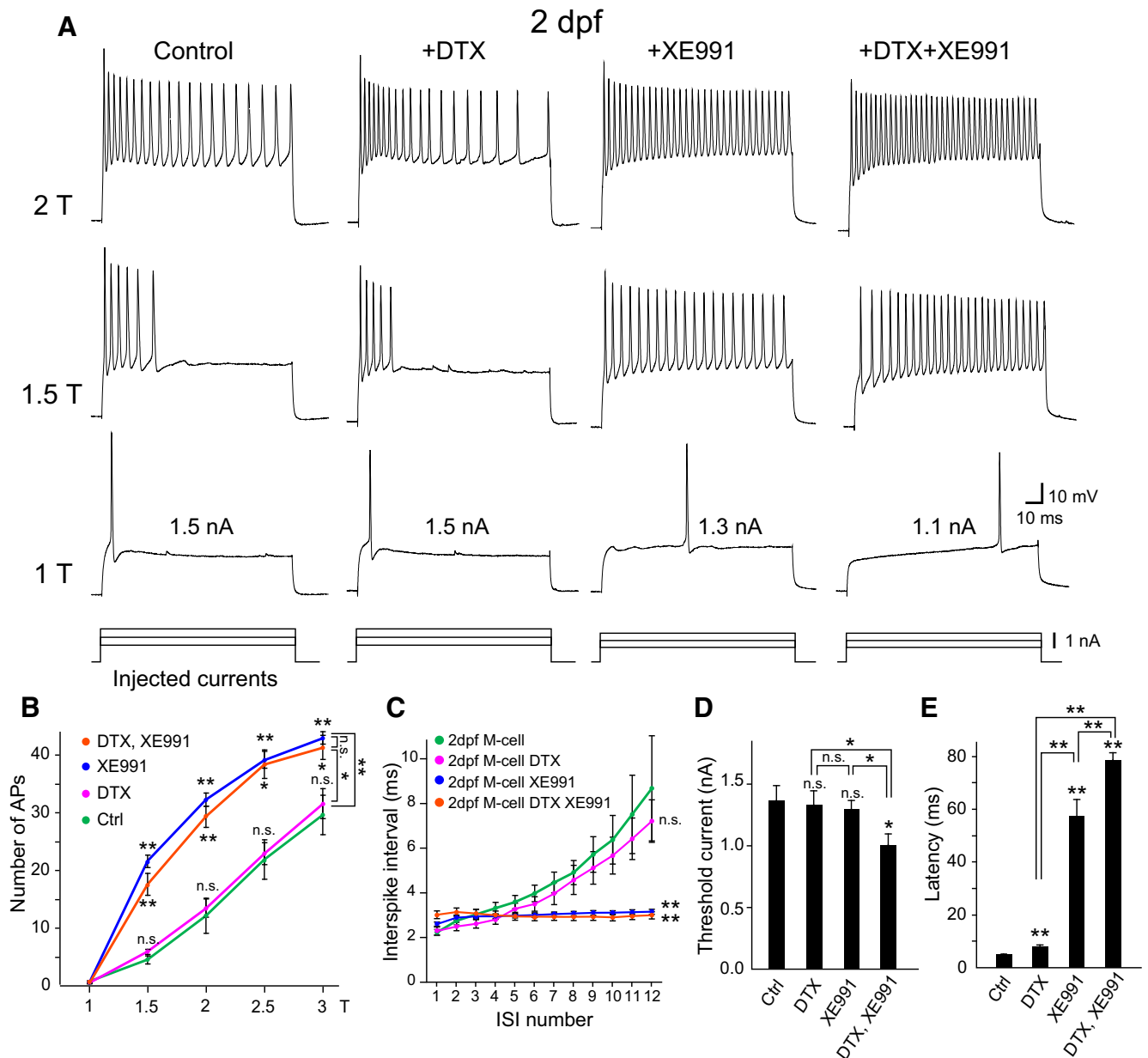


Figure 2. Effect of DTX and/or XE991 on phasic bursting of immature M cells. **A**, Firing response from M cells at 2 dpf. XE991 treatment caused phasic bursting M cells (control) to fire tonically (+XE991, +DTX + XE991), whereas DTX treatment did not (except for a slight delay of spike onset). **B**, Summary graph of the blocker effect at 2 dpf showing that the number of APs elicited during 100-ms current pulses significantly increased after XE991 treatment. **C**, In controls, M cells at 2 dpf showed spike accommodation with a gradual increase in ISI, whereas regular spiking with constant ISI was observed after XE991 treatment. Note that DTX application had no additional effect. **D**, The threshold current was significantly reduced after combined DTX and XE991 treatment. **E**, Spike latency greatly increased after XE991 treatment. n.s., not significant. * $p < 0.05$, ** $p < 0.01$, Mann–Whitney U test (control, $n = 6$; +DTX, $n = 6$; +XE991, $n = 10$; +DTX + XE991, $n = 7$). Two-way repeated measures ANOVA was used for ISI.

were additionally affected by the combined application of DTX and XE991 (Fig. 2D,E).

Overall, these results suggest that Kv7 channels are already expressed in 2-dpf M cells, and that they are required for the establishment of phasic bursting with strong spike-frequency adaptation. Further, this raises the possibility that Kv7 channels are specifically expressed in M cells among M-series neurons.

Kv7.4/KCNQ4 channels are specifically expressed in M cells among M-series neurons

To test this possibility, we investigated the expression of Kv7 channels in M-series neurons during development. In zebrafish, Kv7/KCNQ α -subunit genes consist of *Kv7.1a*, *Kv7.1b*, *Kv7.2a*, *Kv7.2b*, *Kv7.3*, *Kv7.4*, *Kv7.5a*, and *Kv7.5b* (Fig. 3A). Zebrafish Kv7.4 has appeared to consist of two genes in different genomic regions (Wu

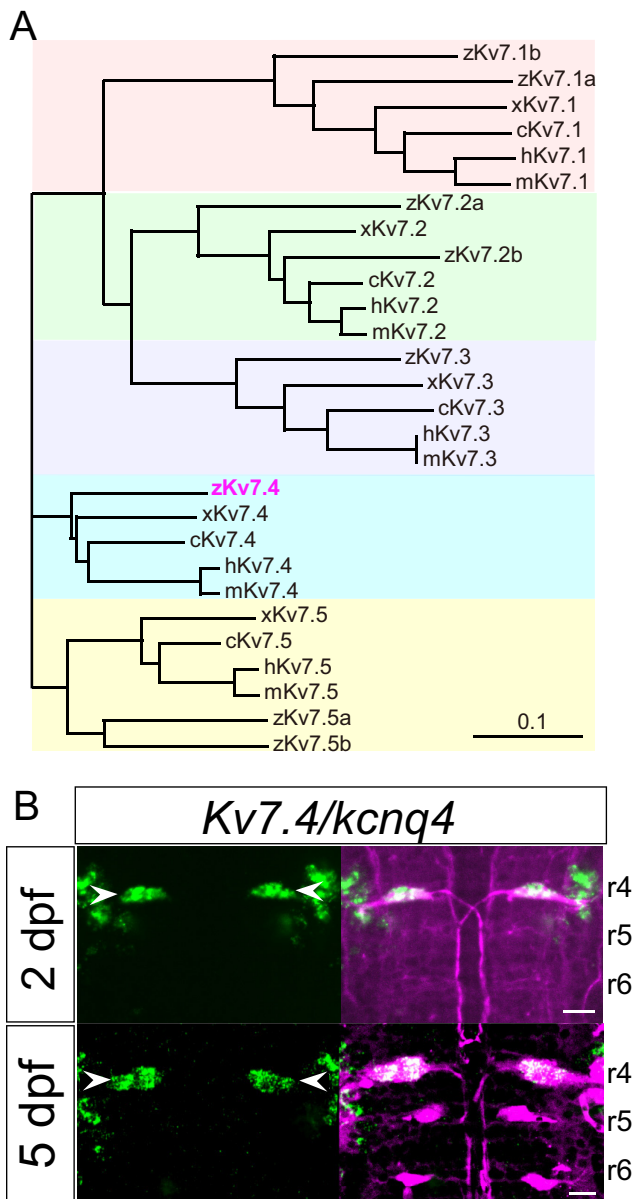


Figure 3. Expression of *Kv7.4/Kcnq4* mRNA in M cells during development. **A**, Phylogenetic tree of α -subunit proteins of XE991-sensitive voltage-gated K^+ channel Kv7/KCNQ family members in zebrafish, *Xenopus*, chick, mouse, and human (z, x, c, m, and h as the gene prefix, respectively), and showing identification of zebrafish Kv7.4 (magenta). **B**, Dorsal views of rhombomeres 4, 5, and 6 (r4, r5, and r6) in the hindbrain at 2 dpf (top) and 5 dpf (bottom) after *in situ* hybridization using a *Kv7.4* antisense probe (green). *Kv7.4* mRNA was expressed in M cells (arrowhead) at 2 and 5 dpf, but not in MiD2cm and MiD3cm cells, labeled (magenta) immunohistochemically (with 3A10 antibody, at 2 dpf) or retrogradely (at 5 dpf). Scale bar, 20 μ m.

et al., 2014). However, due to incomplete genomic sequencing, we were only able to amplify a single full-length *Kv7.4/kcnq4* cDNA segment by RT-PCR from these two genomic regions, in which N- and C-terminal *Kv7.4/kcnq4* are separately located (see Materials and Methods). *In situ* hybridization in 2- and 5-dpf zebrafish revealed that among these genes, only *Kv7.4/kcnq4* mRNA was specif-

ically expressed in M cells, but this expression did not take place in the MiD2cm or MiD3cm (Fig. 3B). In addition, *Kv7.4/kcnq4* mRNA was also expressed in some vestibular neurons located in the lateral M-cell region (Fig. 3B). Other Kv7 subunits were not detected in M-series neurons (data not shown), demonstrating Kv7.4 probe specificity. These results suggest that homomeric Kv7.4 channels are already specifically formed in M cells at 2 dpf, in contrast to Kv1.1 α -subunits (*kcnab1a/Kv1.1a*), which appear in all M-series neurons but exhibit enhanced expression via Kv β 2 (*kcnab2b/Kv β 2b*) auxiliary subunits after 2 dpf (Watanabe et al., 2014).

Zebrafish Kv7.4 channels form low-threshold K^+ currents with slow activation

As demonstrated, Kv7.4 and Kv1.1 channels appear to contribute differentially to the control of M-cell firing. To assess the electrophysiological kinetic differences between the zebrafish Kv7.4 and Kv1.1, we compared voltage-gated currents in *Xenopus* oocytes expressing either of these channels. Zebrafish Kv7.4 channels expressed in oocytes showed slowly-activating outward currents at command voltages above -60 mV (Fig. 4A). The threshold voltage was comparable to that of Kv1.1 (Fig. 4B,C; G/G_{\max} at -60 mV, $p = 0.357$, Mann-Whitney U test; Kv7.4, $n = 20$; Kv1.1a, $n = 32$). However, the rise time of Kv7.4 channel activation was several ten-fold slower than that of Kv1.1 channels (Fig. 4D,E). Interestingly, when coexpressed with auxiliary Kv β 2 subunits, Kv1.1 channel activation was significantly accelerated, with a rise time that was ~ 2 ms faster above -40 mV (Fig. 4E) and an increased current amplitude (Fig. 4B; Watanabe et al., 2014). That these channels have different kinetics is also demonstrated by the half activation voltage ($V_{1/2}$) and slope k parameters of the Boltzmann equation (Table 1). Therefore, the expression of slowly-activating Kv7.4 channels in M cells appears to contribute to strong spike-frequency adaptation in phasic bursting at 2 dpf, and the expression of fast-activating Kv1.1 channels associated with Kv β 2 subunits establishes single spiking after 3 dpf.

Coordinated expression of Kv7.4 and Kv1.1 associated with Kv β 2 underlies developmental differentiation of M-cell excitability among homologous neurons

Next, we examined the role of coexpression of these two low-threshold K^+ channels and Kv β 2 subunits on developmental acquisition of M-cell excitability by examining firing behavior in model cells. We focused on temporal patterns of firing in response to depolarization as well as the latency and threshold of firing. We represented the zebrafish Kv7.4 and Kv1.1 channels with and without Kv β 2 subunits via a basic H-H equation (Fig. 5) and integrated them into a control regular-spiking model (Fig. 6). Voltage-dependent open probability and time-dependent kinetics of the channels were reproduced in the model (Fig. 5B-D, respectively) as observed in the *Xenopus* oocyte system (Fig. 4). It is nearly impossible to precisely determine all of the ionic conductances in M cells via voltage-clamp recording due to large leak cur-

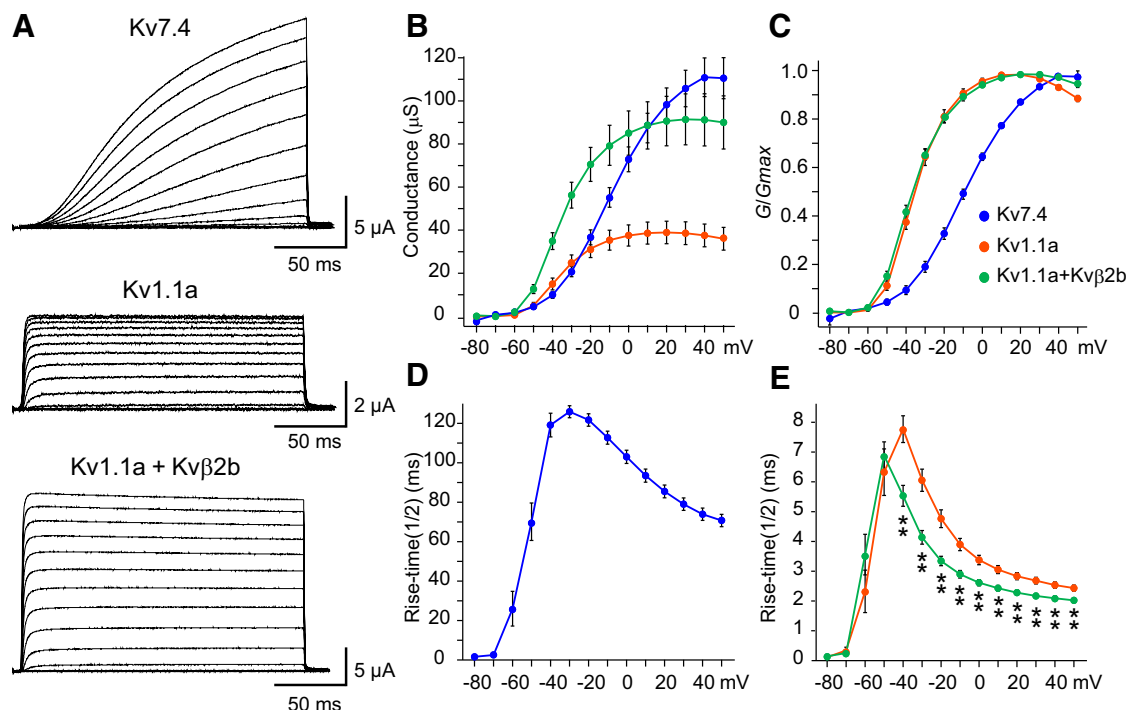


Figure 4. Gating properties of zebrafish Kv7.4 and Kv1.1 with/without Kvβ2 in *Xenopus* oocytes. **A**, Voltage-gated outward currents recorded from *Xenopus* oocytes expressing zebrafish Kv7.4 (top), Kv1.1a alone (middle), or Kv1.1a with Kvβ2b subunit (bottom). Command voltages (V) ranging from -80 to +50 mV in 10 mV steps were applied for 200 ms. **B**, Conductance (G , μS) at peak current amplitude was plotted as a function of the command voltage. **C**, The G -V relationship normalized to maximum value (G_{max}) shows that currents elicited above -60 mV had different open probabilities. **D**, **E**, Rise time to half-maximum activation ($t_{1/2}$) of Kv7.4 (**D**) above -60 mV was significantly different from Kv1.1a with and without Kvβ2b (**E**; $p < 0.01$). $**p < 0.01$, Kruskal-Wallis test with *post hoc* Bonferroni correction (Kv7.4, $n = 20$; Kv1.1a, $n = 32$; Kv1.1a + Kvβ2b, $n = 26$).

rents through gap junctions in huge dendrites (Pereda et al., 2013; Watanabe et al., 2014). Thus, the control

Table 1. Comparison of the parameters of the Boltzmann equation in *Xenopus* oocytes system is shown

	n	$V_{1/2}$ (mV)	k
Kv7.4	20	-10.1 ± 1.7	15.4 ± 0.7
Kv1.1a	32	$-35.4 \pm 1.4^{**}$	$7.4 \pm 0.3^{**}$
Kv1.1a + Kvβ2b	26	$-36.6 \pm 1.1^{**}$	$9.4 \pm 0.5^{**}$

All values are represented as mean \pm SEM. $**p < 0.01$, Mann-Whitney U tests against the value of Kv7.4.

model cell, which reproduces regular spiking as shown by MiD2/3cm (Fig. 1B; Watanabe et al., 2014) or M cells after both DTX and XE991 treatment (Figs. 1, 2), is based on that of mouse cochlear neurons (Rothman and Manis, 2003b). Mouse cochlear neurons express voltage-gated Na^+ channels, high-threshold K^+ channels, and A-type K^+ channels, and fire tonically in response to step depolarization [Fig. 6A; tonic firing ($\bar{g}_{Kv1.1}$, $\bar{g}_{Kv7.4}$: 0, 0)]. The model cells that additionally expressed some degree of Kv1.1 conductance still exhibited tonic firing but at slightly higher frequencies [Fig. 6A; ($\bar{g}_{Kv1.1}$, $\bar{g}_{Kv7.4}$: 150, 0)], as

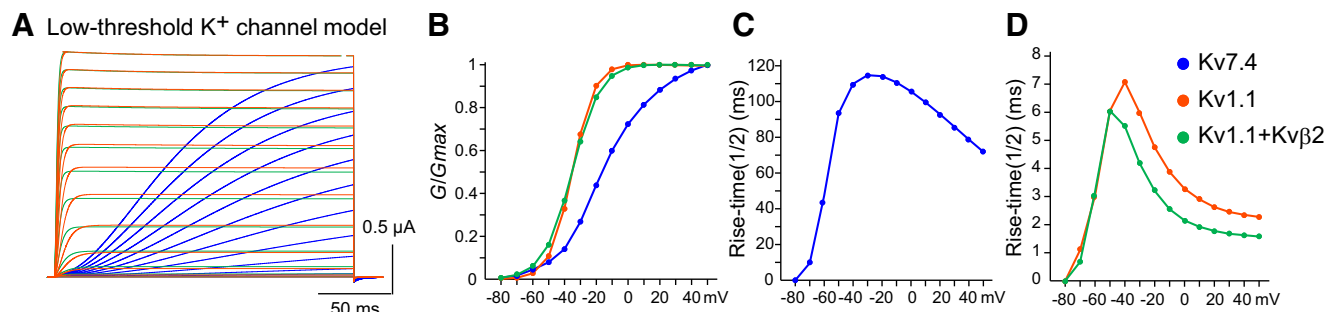


Figure 5. Computational model of low-threshold K^+ channels. **A**, Voltage-gated outward currents of model zebrafish Kv7.4 (blue), Kv1.1 (orange), and Kv1.1 channels coexpressed with Kvβ2 (green) represented by a Hodgkin-Huxley equation. **B**–**D**, Normalized G -V plots (**B**), and rise time ($t_{1/2}$) of model Kv7.4 (**C**), Kv1.1 and Kv1.1 + Kvβ2 (**D**) resemble those obtained in *Xenopus* oocytes (Fig. 4).

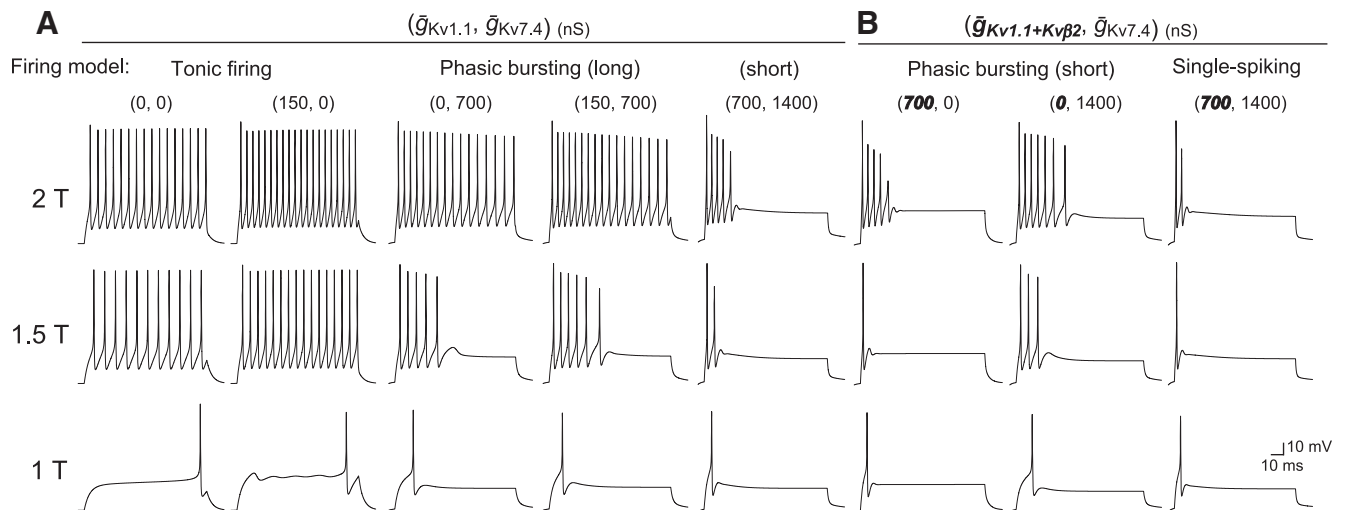


Figure 6. M-cell firing model integrating low-threshold K^+ channels in response to long step currents. **A**, **B**, Representative current-clamp simulation of a model neuron integrating two types of low-threshold K^+ channels associated with Kv β 2 subunits into a basic tonic-firing model. Long step currents of 1T, 1.5T, and 2T were injected. Maximum conductances ($\bar{g}_{Kv1.1}$, $\bar{g}_{Kv7.4}$; **A**) or ($\bar{g}_{Kv1.1+Kv\beta 2}$, $\bar{g}_{Kv7.4}$; **B**) are indicated in parentheses. Bold italic numbers represent conductances associated with Kv β 2. Expression of low-threshold K^+ channels alters the tonic-firing model to exhibit phasic bursting with long or short firing duration and single spiking, as observed with *in vivo* M-cell recordings (Figs. 1, 2).

observed in 2-dpf M cells after XE991 treatment. Integration of both Kv1.1 and Kv7.4 conductance ($\bar{g}_{Kv1.1}$, $\bar{g}_{Kv7.4}$: 150, 700) and Kv7.4 conductance only ($\bar{g}_{Kv1.1}$, $\bar{g}_{Kv7.4}$: 0, 700) reproduced phasic bursting of M cells at 2 dpf and those after DTX treatment, respectively [Fig. 6A; phasic bursting (long)]. The spike latency increased when the Kv1.1 conductance was subtracted from the 2-dpf M-cell model, as observed after DTX treatment. To test the effect of Kv β 2 subunit coexpression on firing, we increased the model Kv1.1 conductance along with an acceleration in activation kinetics of ~ 2 ms above -40 mV ($\bar{g}_{Kv1.1+Kv\beta 2}$: 700), as observed in oocytes (Figs. 5D, 6B). The model cell with either enhanced Kv1.1 conductance with Kv β 2 or twice as many Kv7.4 channels showed phasic bursting [Fig. 6B; phasic bursting (short) ($\bar{g}_{Kv1.1+Kv\beta 2}$, $\bar{g}_{Kv7.4}$: 700, 0 or 0, 1400)]. The model cell exhibited single spiking only when both conductances were integrated [Fig. 6B; single spiking ($\bar{g}_{Kv1.1+Kv\beta 2}$, $\bar{g}_{Kv7.4}$: 700, 1400)]. The model cell ($\bar{g}_{Kv1.1}$, $\bar{g}_{Kv7.4}$: 700, 1400) expressing the two channels but without acceleration by Kv β 2 still exhibited short phasic bursting activated by a lower threshold current [Fig. 6A; phasic bursting (short)]. These simulations demonstrate that the coordinated expression of Kv7.4 and Kv1.1 coexpressed with Kv β 2 accounts for the developmental change in M-cell excitability from phasic long bursting at 2 dpf to single spiking at 4 dpf. Moreover, Kv7.4 conductance appears to increase during M-cell development (see Discussion).

In addition to the typical examples above, we comprehensively analyzed the relationship between the amount of low-threshold K^+ conductance and model cell excitability, as shown in Figure 7. While recruitment of Kv1.1 conductance in tonic-firing cells increased the threshold current and shortened the firing onset latency, especially when coexpressed with Kv β 2, the addition of Kv7.4 conductance had a relatively small effect (Fig. 7A,B). Increas-

ing Kv7.4 conductance resulted in a gradual suppression of bursting (Fig. 7C,D) accompanied by strong spike-frequency adaptation (Fig. 7E; ordinate), while increasing Kv1.1 conductance had a relatively small effect (Fig. 7E; abscissa). Thus, Kv7.4 and Kv1.1 channels play distinct firing property roles, while Kv β 2 subunits enhance the effect of Kv1.1 channels. It should be noted that Kv β 2 coexpression had a significant impact on phasic firing, even at smaller conductances.

We represented behaviors of different types of voltage-gated channels during phasic firing of M cells using the model cell (Fig. 8). During phasic bursting, Kv1.1 channels are periodically activated from the onset of current injection, whereas activation of Kv7.4 channels is gradually increased at the later phase of repetitive firing (Fig. 8A,B; red vs blue). Thus, fast activation of Kv1.1 channels with low density presumably increases firing frequency rather than suppressing later firing, whereas slow activation of Kv7.4 channels mainly affects spike-frequency adaptation. In the case of single spiking, activation of Kv1.1 with Kv β 2 rose rapidly immediately at onset, and maintained high levels until the end of spiking. In contrast, Kv7.4 activation increased gradually for phasic bursting (Fig. 8C,D). These data suggest that the fast activation and high conductance of Kv1.1 channels coexpressed with Kv β 2 strongly inhibits bursting after the first AP. Further, at juxta-threshold voltages, Kv1.1 with Kv β 2 also contributed to fast activation of voltage-gated Na^+ conductance, whereas Kv7.4 did not (Fig. 8E–H). The differing contribution of Kv1.1 channels with Kv β 2 and Kv7.4 channels on Na^+ channels may underlie the differences in spike latency of M cells during DTX and XE991 treatment.

Finally, we estimated a role for the expression of the two K^+ channels on M cells in the firing response to auditory inputs by applying repetitive short-pulse depolarizing currents (0.5 ms, 0–3 nA) at 500 Hz (Fig. 9).

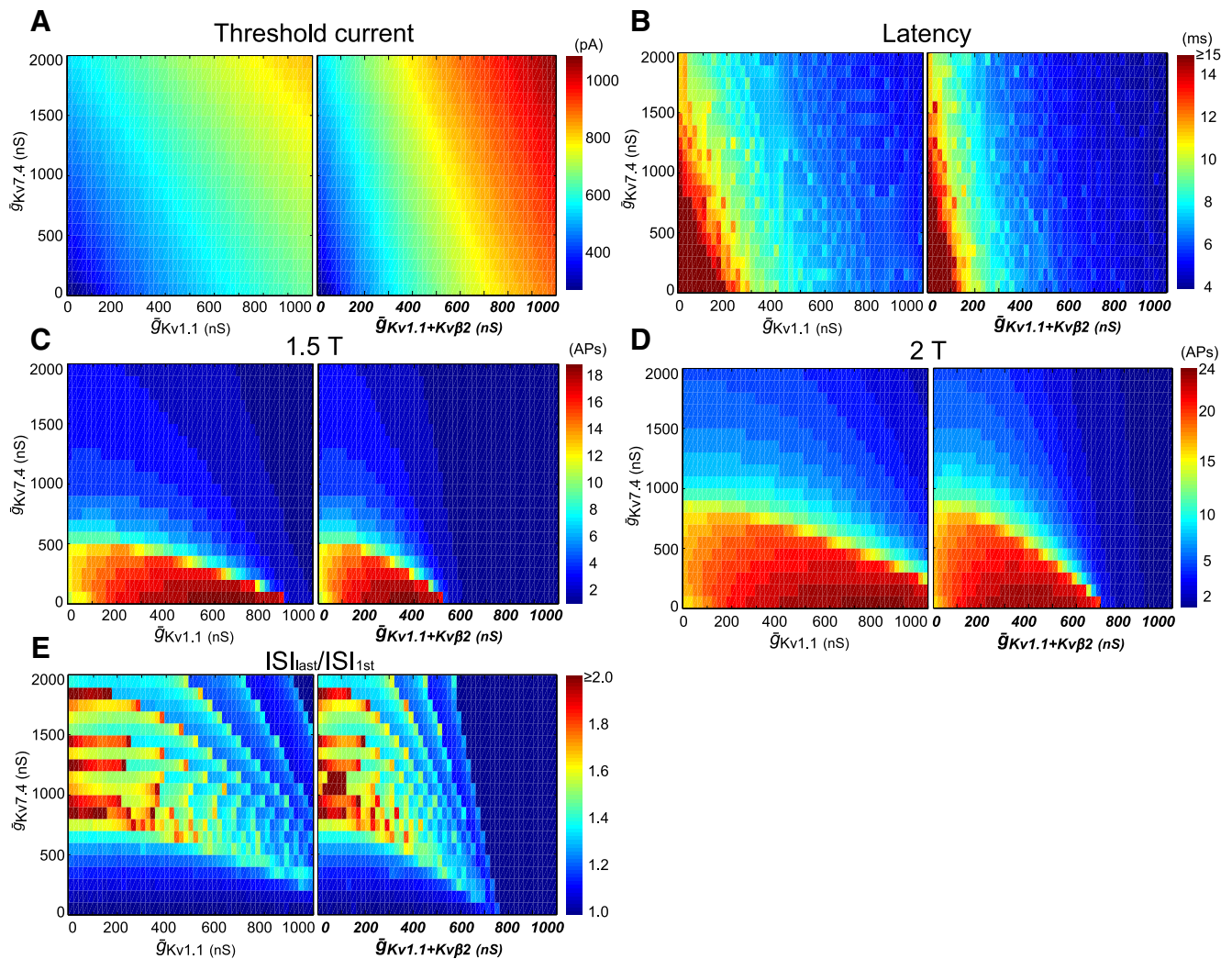


Figure 7. Comprehensive analysis of firing parameters in the M-cell model. **A–E**, Firing parameters of low-threshold K^+ channel-integrated model cells with different combinations of ($\bar{g}_{Kv1.1}$, $\bar{g}_{Kv7.4}$; left) or ($\bar{g}_{Kv1.1+Kv\beta2}$, $\bar{g}_{Kv7.4}$; right), with respect to threshold current (T; **A**), onset latency of first AP at 1T (**B**), number of elicited APs during 100 ms at 1.5T (**C**) and 2T (**D**), and ISI_{last}/ISI_{1st} at 2T (**E**). In each panel, 1071 firing patterns (21×51 combinations) were produced by increments of 100 ns for $\bar{g}_{Kv7.4}$ and 20 ns for $\bar{g}_{Kv1.1}$ or $\bar{g}_{Kv1.1+Kv\beta2}$, ranging from 0–2000 ns (40 ms/cm²) and 0–1000 ns (20 ms/cm²), respectively. The Kv1.1 model ($\bar{g}_{Kv1.1}$, $\bar{g}_{Kv7.4}$: 480, 0) and Kv1.1 + Kv β 2 model ($\bar{g}_{Kv1.1+Kv\beta2}$, $\bar{g}_{Kv7.4}$: 240, 0) had a similar threshold current (around 500 pA; **A**). The Kv1.1 model ($\bar{g}_{Kv1.1}$, $\bar{g}_{Kv7.4}$: 920, 0) showed two spikes at 1.5T, and this firing rate was also seen in the Kv1.1 + Kv β 2 model ($\bar{g}_{Kv1.1+Kv\beta2}$, $\bar{g}_{Kv7.4}$: 540, 0; **C**), indicating that faster activation of Kv1.1 by Kv β 2 efficiently suppressed repetitive firing.

M-series neurons receive direct auditory afferent nerves that burst at 100–1000 Hz in goldfish (Fay, 1995). Firing responses of the model ($\bar{g}_{Kv1.1}$, $\bar{g}_{Kv7.4}$) or ($\bar{g}_{Kv1.1+Kv\beta2}$, $\bar{g}_{Kv7.4}$) were quite similar to those evoked by step current injection (Figs. 6, 9A,B). A tonic firing model [$\bar{g}_{Kv1.1}$, $\bar{g}_{Kv7.4}$: 0, 0 or 150, 0] quickly increased firing frequency just above the threshold currents, whereas a phasic bursting model [$\bar{g}_{Kv1.1}$, $\bar{g}_{Kv7.4}$: 0, 700 or 150, 700] gradually increased the number of APs with a lower frequency in a range of relatively small intensities above the threshold (Fig. 9A,C). A single-spiking model [$\bar{g}_{Kv1.1+Kv\beta2}$, $\bar{g}_{Kv7.4}$: 700, 1400] generated a single AP in response to large current intensities (2.5–3 nA), while a short phasic-bursting model [$\bar{g}_{Kv1.1+Kv\beta2}$, $\bar{g}_{Kv7.4}$: 700, 0 or 0, 1400] produced repetitive firing with a high frequency in response to the same large current intensities (Fig. 9B,D).

The effects of integration of these channels on threshold current and latency of the first AP had the same tendency for both M cells *in vivo* (Fig. 1, 2) and those in the simulation with step current injection (Figs. 6, 9E,F).

Taken together, these results demonstrate that coordinated expression of slowly-activating Kv7.4 channels, fast-activating Kv1.1 channels, and enhancement by auxiliary Kv β 2 subunits produces heterogeneity of phasic firing in M cells with different developmental stages, thus further differentiating these neurons from homologous counterparts.

Discussion

Using the zebrafish as a model to understand how unique single spiking is produced based on a tonic-firing property, we have identified ionic mechanisms underlying

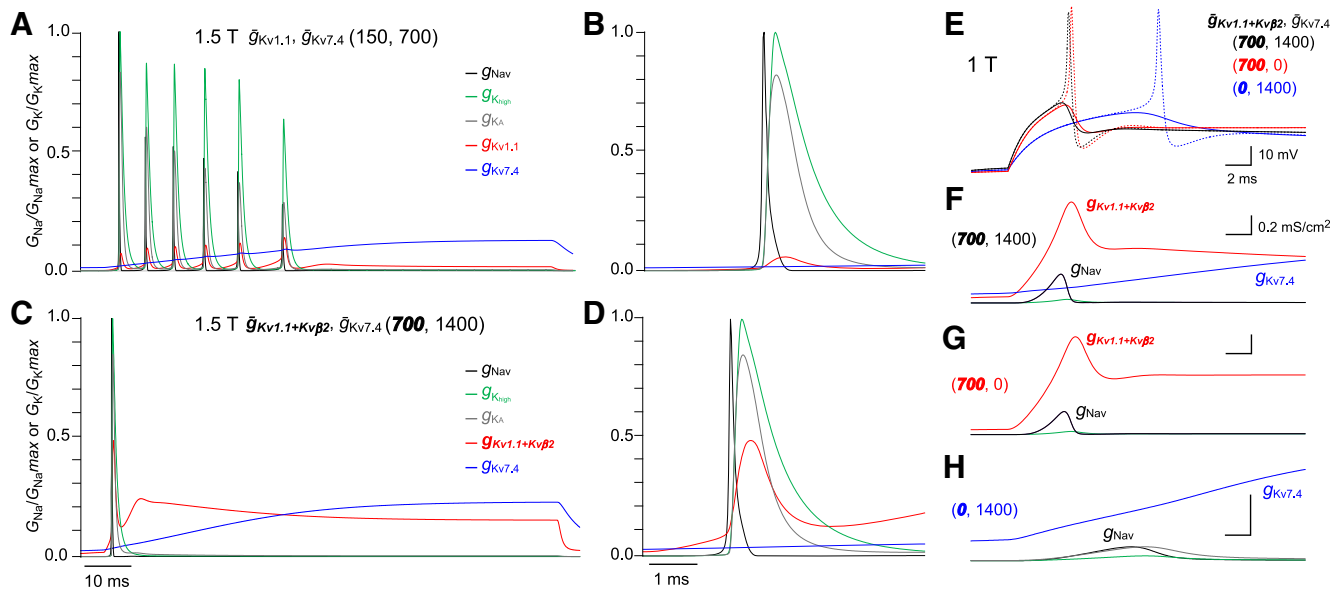


Figure 8. Na^+ and K^+ conductance mechanisms for producing characteristic phasic properties. **A–D**, Representative dynamics of voltage-gated Na^+ and K^+ channel conductance for g_{Nav} (black), g_{high} (green), g_{A} (gray), $g_{\text{Kv7.4}}$ (blue), and $g_{\text{Kv1.1}}$ or $g_{\text{Kv1.1+Kv}\beta 2}$ (red) during current-clamp stimulation. These conductances were normalized to maximum values of Na^+ or among K^+ conductance at 1.5T using a 2-dpf (**A, B**) and 4-dpf (**C, D**) M-cell model, shown in Figure 7A,B, respectively. Conductance dynamics at the beginning of current injection in **B, D** show the first AP generation of **A, C**, respectively. **E–H**, Changes in membrane potential at subthreshold (solid line, below 1–2 pA of 1T), and 1T (dashed line) in the 4-dpf M-cell model (black), XE991-treated model (red), and DTX-treated model (blue; **E**). The corresponding Na^+ and K^+ conductance in each model during subthreshold firing (**F–H**). Na^+ conductance became much larger after fast activation of K^+ conductance ($\bar{g}_{\text{Kv1.1+Kv}\beta 2}$; **F, G**) compared with slow activation of K^+ conductance ($\bar{g}_{\text{Kv7.4}}$; **H**).

developmental differentiation of M-cell excitability among segmentally homologous hindbrain neurons. Single-spiking mature M cells begin to fire tonically, as observed in the M-cell homologs, when two types of low-threshold K^+ currents are blocked (Fig. 1), indicating that the ionic basis for tonic firing is conserved in the M series. Conversely, these low-threshold K^+ currents are responsible for differentiation of M-cell excitability from that of the M-cell homologs. In contrast to common Kv1.1 channel expression among the M series (Watanabe et al., 2014), slowly-activating Kv7.4 channels and auxiliary Kv β 2 subunits that accelerate and increase Kv1.1 currents are expressed specifically in M cells from embryonic and later developmental stages, respectively. The expression of Kv7.4 channels and Kv β 2 associated-Kv1.1 channels during development plays different roles in phasic firing such that the combination of these activities induces M cells to acquire their characteristic single-spiking pattern.

Other mechanisms are known to generate phasic or single spiking properties. A change in intrinsic membrane properties from tonic to phasic firing has been well investigated in spiny lobster culture preparations of stomatogastric ganglion neurons, which can be accounted for by increased Ca^{2+} currents and decreased K^+ currents (Turrigiano et al., 1994; Turrigiano et al., 1995). In rat ventral horn neurons, pharmacological blocking of persistent Na^+ currents causes tonic-firing neurons to fire a single spike (Theiss et al., 2007). Simulation analysis of RSNs in frog tadpoles suggests that single spiking evoked by step current injection is not a cellular property but the consequence of a shunting effect resulting from electrical cou-

pling via gap-junction connections among a neural population (Hull et al., 2015). Because we did not test the contribution of these currents to M-cell firing, we cannot exclude the possibility that Ca^{2+} currents, persistent Na^+ currents, and gap-junction connections might underlie M-cell firing properties. However, even if they exist in M cells, their contribution will presumably only have a minimal effect on generating single spiking of M cells because of the necessity and sufficiency of coexpression of the two low-threshold K^+ channels for single spiking.

Coexpression of Kv7.4 and Kv1.1 channels in vertebrate sensory neurons

Which neurons express both Kv7 and Kv1 channels, like M cells, in vertebrates? In zebrafish, vestibular nucleus neurons express Kv7.4 and Kv1.1 channels from 2 dpf, and Kv β 2 subunits from 5 dpf (Fig. 3B; Watanabe et al., 2014). In rat vestibular ganglion neurons both Kv7 and Kv1 channels are required for single-spiking vestibular afferent neurons (Kalluri et al., 2010), which express K^+ channels including Kv7.4 and/or Kv1.1 (Hurley et al., 2006; Lysakowski et al., 2011). Interestingly, phasic spiral ganglion neurons located at the base of the cochlea exhibit stronger expression of Kv7.4 and/or Kv1.1 than tonic neurons located at the apex (Beisel et al., 2000; Adamson et al., 2002). Furthermore, coexpression of Kv7 and Kv1 channels associated with Kv β subunits has been indirectly suggested not only in vestibular and auditory neurons but also phasic trigeminal ganglia neurons and dorsal root ganglia neurons, as well as their secondary sensory neurons, in mice and rats (Rhodes et al., 1996;

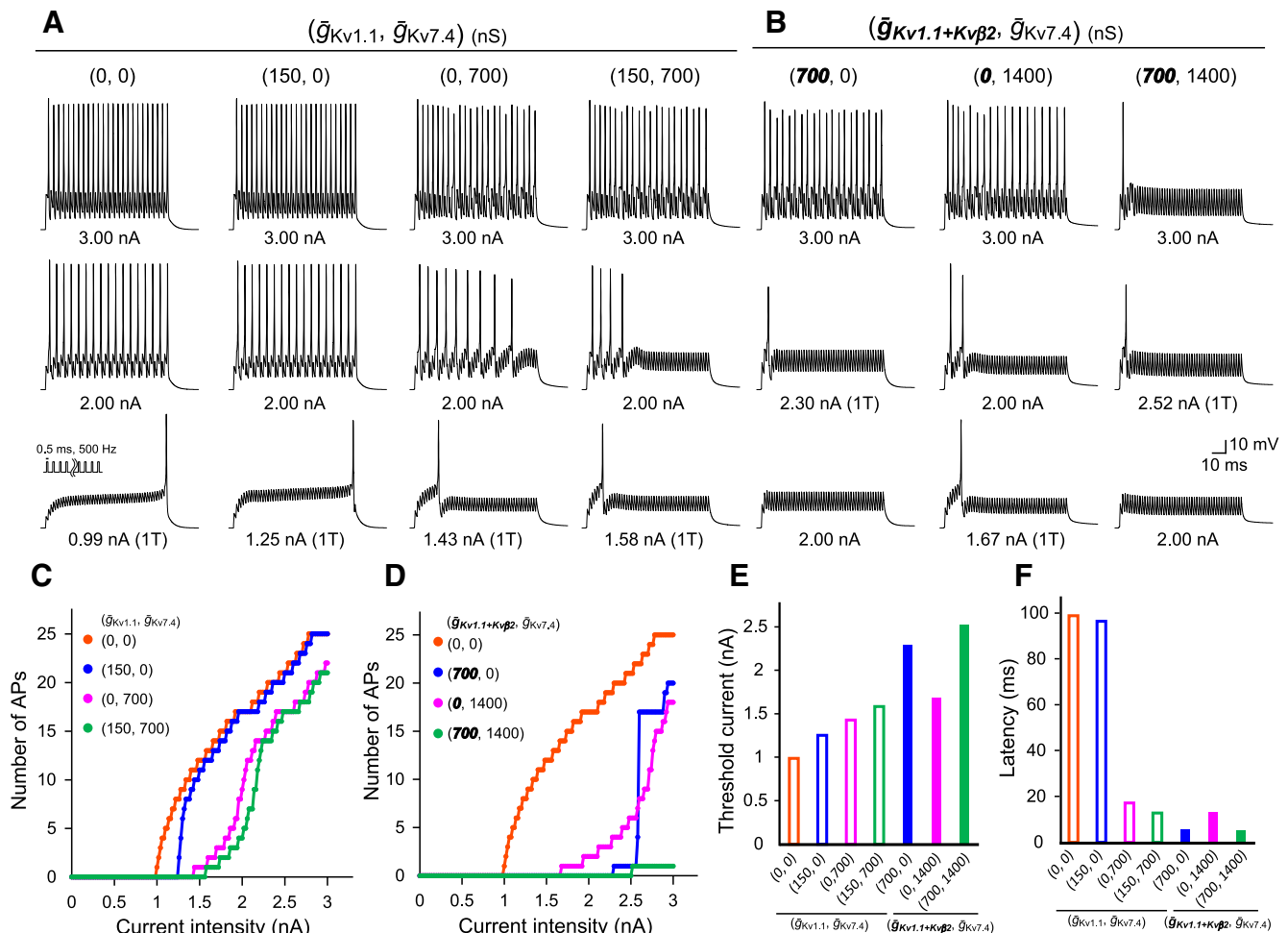


Figure 9. Simulation of M-cell firing in response to repetitive short-pulse currents. **A, B**, Current-clamp simulation of each model neuron ($\bar{g}_{Kv1.1}, \bar{g}_{Kv7.4}$; **A**) or ($\bar{g}_{Kv1.1+Kv\beta2}, \bar{g}_{Kv7.4}$; **B**), which was the same as in Figure 6 except that repetitive short-pulse currents (0.5 ms) of 1T, 2 nA, and 3 nA with 500 Hz were given for 100 ms. **C, D**, Number of APs simulated in ($\bar{g}_{Kv1.1}, \bar{g}_{Kv7.4}$; **C**) or ($\bar{g}_{Kv1.1+Kv\beta2}, \bar{g}_{Kv7.4}$; **D**) are plotted during the current injection in 20-pA increments up to 3 nA. **E, F**, Threshold current (**E**) and onset latency of the first spike at 1T (**F**) for each model neuron ($\bar{g}_{Kv1.1}, \bar{g}_{Kv7.4}$) or ($\bar{g}_{Kv1.1+Kv\beta2}, \bar{g}_{Kv7.4}$).

Kharkovets et al., 2000; Rasband et al., 2001; Caminos et al., 2005; Heidenreich et al., 2012). Thus, coordinated expression of two types of low-threshold K^+ channels is observed in the vertebrate sensory system.

Kv7.4 gene mutations in humans and mice lead to impairments of hearing and touch sensation caused by dysfunction and progressive degeneration of outer hair cells (Kharkovets et al., 2006) or disruption of phasic neurons in trigeminal and dorsal root ganglia (Heidenreich et al., 2012). Kv1.1 mutations in humans and knock-out in mice are known to cause episodic ataxia type 1 associated with epilepsy, which results from dysfunction of the cerebellum, hippocampus, cortex, and peripheral nervous system (Smart et al., 1998; D'Adamo et al., 2015). In the auditory system of Kv1.1 knock-out mice, phasic firing of the ventral cochlear nucleus and medial nucleus of trapezoid body neurons impairs temporal spiking precision and increases firing frequency (Brew et al., 2003; Kopp-Scheinpflug et al., 2003; Gittelmann and Tempel, 2006), causing reduced performance of interaural intensity difference in the lateral superior olive (Karcz et al., 2011).

These findings demonstrate that losing either of two low-threshold K^+ channels in sensory neurons results in sensory dysfunction by altering phasic neurons to display hyperexcitability or loss of temporal precision. Therefore, coordinated expression in these neurons appears to play a crucial role in detecting phasic or onset timing and raising the firing threshold against sensory stimuli, as likely in the case of M cells. To reveal the physiologic role of these channels in M cell-initiated escape behavior, further behavioral experiments combined with M cell-specific gene manipulation of these channels is needed.

Distinct roles of Kv7.4 and Kv1.1 channels in phasic-firing properties

Previous computational model studies have reconstructed phasic-firing patterns by implementing either Kv1 channels (Rothman and Manis, 2003b; Catacuzzeno et al., 2008) or Kv7 channels (Zaika et al., 2006) in tonic-firing cells. Here, as the cochlear nucleus neuron model (Rothman and Manis, 2003a), our model also indicated

that the suppression of repetitive firing by Kv1.1 channels alone requires large conductance (Fig. 7C,D).

Slowly-activating Kv7.4 channels work primarily via spike-frequency adaptation to produce shorter bursts at frequencies that increase with injected currents (Figs. 6, 7). This role for Kv7/KCNQ channels in spike-frequency adaptation has been emphasized in rat sympathetic neurons and mouse CA1 pyramidal neurons, in which heteromeric channels composed of Kv7.2/KCNQ2 and Kv7.3/KCNQ3 subunits are expressed (Wang et al., 1998; Chung et al., 2006; Soh et al., 2014). Phasic-bursting neurons in the mouse cerebral cortex also exhibit firing with frequencies proportional to input intensity and longer onset spike latency, i.e., over 10 ms (Soh et al., 2014). Thus, neurons expressing only Kv7 channels in addition to conventional voltage-gated Na^+ and high-threshold K^+ channels burst phasically with spike-frequency adaptation, as is the case with M cells at 2 dpf.

Here, for the first time, we have shown the necessity of integrated expression of Kv7.4 channels and Kv1.1 channels with Kv β 2 auxiliary subunits to produce single spiking as the most extreme pattern of phasic firing. Further, fast outward currents through the Kv1.1 channels substantially increased the threshold current for spiking, as reported before in rat vestibular neurons (Kalluri et al., 2010). Kv1.1 channels associated with Kv β 2 shortened the spike latency (Figs. 6, 7, 9). Therefore, neurons expressing Kv1 channels associated with Kv β 2 encode onset-timing information in response to relatively large inputs, but still burst at an input intensity-dependent frequency [Figs. 6B, 9B; phasic bursting (short)]. Together, neurons expressing both Kv7 and Kv β 2-associated Kv1 channels extract precise onset-timing information without duration and intensity, as is the case with M cells and rat vestibular neurons (Kohashi and Oda, 2008; Kalluri et al., 2010).

The effect of combined DTX and XE991 treatment was greater than either treatment at 2 and 4 dpf in M cells (Figs. 1F, 2E), and this phenomenon was replicated in model cells (Figs. 7B, 8E–H, 9F). Thus, in addition to Kv1, Kv7 currents also shorten spike latency but the effect is much smaller than Kv1 currents. This difference may be mainly due to the distinct impact on Na^+ conductance activation (Fig. 8E–H). Faster activation of Na^+ conductance may be attributed to reduced membrane resistance and a shorter time constant of the depolarizing phase before spiking, which is caused by rapidly increasing K^+ currents from Kv1.1 channels associated with Kv β 2 rather than slowly-activating Kv7.4 channels. Conversely, without low-threshold K^+ currents, the membrane depolarization time constant becomes much longer (as passive membranes demonstrate), and then a slower depolarization only weakly activates Na^+ conductance, resulting in a considerably longer spike latency of tonic firing.

Developmental increases in Kv7.4 and Kv1.1 conductance

Our comprehensive simulation produced pairs of conductances for low-threshold K^+ channels that best explain our experimental data, with a relatively higher

conductance for Kv7.4 versus Kv1.1 (Fig. 6). The higher Kv7.4 conductance presumably originated from incomplete modification of basic H-H models of g_{Nav} , g_{high} , and g_{A} based on cochlear neurons (Rothman and Manis, 2003b) along with the differences in voltage range and rise time for activation of Kv7.4 versus Kv1.1 channels (Fig. 4). Our modifications of g_{Nav} , g_{high} , and g_{A} were arbitrarily adjusted by fitting model firing and AP wave form to experimental data of 4-dpf M cells, which somehow affected our model results throughout development. A comparison between the zebrafish Kv7.4 and the other Kv7 channels in the mouse indicated that zebrafish Kv7.4 channels have more depolarized $V_{1/2}$ parameters compared with mouse KCNQ1, KCNQ2 and KCNQ4 channels (Nakajo and Kubo, 2005). This suggests that these channels play different roles in zebrafish M cells and mouse neurons.

Our M-cell model indicated that increasing the Kv7.4 and Kv1.1 currents by 2 and 4.7 times, respectively, sufficiently reproduced M-cell development and data from previous pharmacological studies. Increases in Kv1.1 currents can be explained by enhanced surface expression associated with Kv β 2, as observed in the *Xenopus* oocyte system (Fig. 5), and/or possibly by developmental accumulation of gene expression in M cells. Indeed, this increase in gene expression corresponds to the development of auditory and vestibular neurons in mammals and birds, and these neurons can alter intrinsic firing properties in response to increases in Kv1 currents and expression levels (Gamkrelidze et al., 1998; Nakamura and Takahashi, 2007; Iwasaki et al., 2008; Iwasaki et al., 2012). Alternatively, the molecular basis for the developmental increases in Kv7.4 conductance may not simply be explained by an increase in gene expression, because strong expression was already observed at 2 dpf (Fig. 3B).

What possible mechanisms underlie the increase of Kv7.4 currents? Alternative splicing variants in mouse Kv7.4/KCNQ4 (variants 1–4) exhibit distinct current amplitudes when expressed in Chinese hamster ovarian cells (Xu et al., 2007). These isoforms are differentially expressed in inner hair cells, afferent spiral ganglion neurons (Beisel et al., 2005), and vestibular ganglion neurons (Rocha-Sanchez et al., 2007), suggesting nervous system regulation of conductance by Kv7.4 isoforms. Moreover, mammalian Kv7 conductance is modulated and inhibited by phosphorylation of C-terminal sites via protein kinase C (PKC; Hoshi et al., 2003; Nakajo and Kubo, 2005). Further, membrane surface expression and kinetics are regulated by association with potassium voltage-gated channel subfamily E (KCNE) β -subunits (KCNE1–5; Strutz-Seeböhm et al., 2006; Pongs and Schwarz, 2010). In this study, we found that the zebrafish Kv7.4 is comparable to a short-type variant of the mouse homolog, with conserved PKC-phosphorylated residues in the C terminus, shown by amino acid sequence alignment across vertebrates (Fig. 3A; Nakajo and Kubo, 2005). M cells express PKC γ protein, at least from 2 dpf (Patten et al., 2007). Zebrafish KCNE1 and KCNE4 subunits are present in the zebrafish genome database (Zv9), but not all homologs have been identified. Further studies are

required to examine possible changes in splicing isoform expression, and to determine if regulation of Kv7.4 channels via PKC or KCNE β -subunits is involved in M-cell excitability during development.

In conclusion, M-series neurons may represent the simplest model for explaining the developmental establishment of different phasic-firing properties from a tonic-firing property in a neural population via coordinated expression of low-threshold K⁺ channel subunits. Because Kv1, Kv β , and Kv7 gene families are widely expressed in the vertebrate nervous system, it is likely that distinct activation-kinetics and expression or conductance levels of these low-threshold K⁺ channels play important roles in producing heterogeneity of phasic-firing properties.

References

- Adamson CL, Reid MA, Mo ZL, Bowne-English J, Davis RL (2002) Firing features and potassium channel content of murine spiral ganglion neurons vary with cochlear location. *J Comp Neur* 447:331–350. [CrossRef Medline](#)
- Beisel KW, Nelson NC, Delimont DC, Fritsch B (2000) Longitudinal gradients of KCNQ4 expression in spiral ganglion and cochlear hair cells correlate with progressive hearing loss in DFNA2. *Brain Res Mol Brain Res* 82:137–149. [Medline](#)
- Beisel KW, Rocha-Sanchez SM, Morris KA, Nie L, Feng F, Kachar B, Yamoah EN, Fritsch B (2005) Differential expression of KCNQ4 in inner hair cells and sensory neurons is the basis of progressive high-frequency hearing loss. *J Neurosci* 25:9285–9293. [CrossRef Medline](#)
- Brew HM, Forsythe ID (1995) Two voltage-dependent K⁺ conductances with complementary functions in postsynaptic integration at a central auditory synapse. *J Neurosci* 15:8011–8022.
- Brew HM, Hallows JL, Tempel BL (2003) Hyperexcitability and reduced low threshold potassium currents in auditory neurons of mice lacking the channel subunit Kv1.1. *J Physiol* 548:1–20. [CrossRef Medline](#)
- Caminos E, Vale C, Lujan R, Martinez-Galan JR, Juiz JM (2005) Developmental regulation and adult maintenance of potassium channel proteins (Kv 1.1 and Kv 1.2) in the cochlear nucleus of the rat. *Brain Res* 1056:118–131. [CrossRef Medline](#)
- Cardin JA, Carlén M, Meletis K, Knoblich U, Zhang F, Deisseroth K, Tsai LH, Moore CI (2009) Driving fast-spiking cells induces gamma rhythm and controls sensory responses. *Nature* 459:663–667. [CrossRef Medline](#)
- Carr CE, Soares D (2002) Evolutionary convergence and shared computational principles in the auditory system. *Brain Behav Evol* 59:294–311. [Medline](#)
- Catacuzzeno L, Fioretti B, Pietrobon D, Franciolini F (2008) The differential expression of low-threshold K⁺ currents generates distinct firing patterns in different subtypes of adult mouse trigeminal ganglion neurones. *J Physiol* 586:5101–5118. [CrossRef Medline](#)
- Chung HJ, Jan YN, Jan LY (2006) Polarized axonal surface expression of neuronal KCNQ channels is mediated by multiple signals in the KCNQ2 and KCNQ3 C-terminal domains. *Proc Natl Acad Sci USA* 103:8870–8875. [CrossRef Medline](#)
- D'Adamo MC, Hasan S, Guglielmi L, Servettini I, Cenciarini M, Catacuzzeno L, Franciolini F (2015) New insights into the pathogenesis and therapeutics of episodic ataxia type 1. *Front Cell Neurosci* 9:317
- Fay RR (1995) Physiology of primary saccular afferents of goldfish: implications for Mauthner cell response. *Brain Behav Evol* 46:141–150. [Medline](#)
- Gamkrelidze G, Giaume C, Peusner KD (1998) The differential expression of low-threshold sustained potassium current contributes to the distinct firing patterns in embryonic central vestibular neurons. *J Neurosci* 18:1449–1464. [Medline](#)
- Gittelman JX, Tempel BL (2006) Kv1.1-containing channels are critical for temporal precision during spike initiation. *J Neurophysiol* 96:1203–1214. [CrossRef Medline](#)
- Heidenreich M, Lechner SG, Vardanyan V, Wetzel C, Cremers CW, De Leenheer EM, Aránguez G, Moreno-Pelayo MA, Jentsch TJ, Lewin GR (2012) KCNQ4 K(+) channels tune mechanoreceptors for normal touch sensation in mouse and man. *Nat Neurosci* 15:138–145. [CrossRef Medline](#)
- Hines ML, Carnevale NT (2001) NEURON: a tool for neuroscientists. *Neuroscientist* 7:123–135. [CrossRef Medline](#)
- Hoffpauir BK, Kolson DR, Mathers PH, Spirou GA (2010) Maturation of synaptic partners: functional phenotype and synaptic organization tuned in synchrony. *J Physiol* 588:4365–4385. [CrossRef Medline](#)
- Hopkins WF, Allen ML, Houamed KM, Tempel BL (1994) Properties of voltage-gated K⁺ currents expressed in *Xenopus* oocytes by mKv1.1, mKv1.2 and their heteromultimers as revealed by mutagenesis of the dendrotoxin-binding site in mKv1.1. *Pflugers Arch* 428:382–390. [Medline](#)
- Hoshi N, Zhang JS, Omaki M, Takeuchi T, Yokoyama S, Wanaverbecq N, Langeberg LK, Yoneda Y, Scott JD, Brown DA, Higashida H (2003) AKAP150 signaling complex promotes suppression of the M-current by muscarinic agonists. *Nat Neurosci* 6:564–571. [CrossRef Medline](#)
- Hull MJ, Soffe SR, Willshaw DJ, Roberts A (2015) Modelling the effects of electrical coupling between unmyelinated axons of brainstem neurons controlling rhythmic activity. *PLoS Comput Biol* 11:e1004240. [CrossRef Medline](#)
- Hurley KM, Gaboyard S, Zhong M, Price SD, Wooltorton JR, Lysakowski A, Eatock RA (2006) M-like K⁺ currents in type I hair cells and calyx afferent endings of the developing rat utricle. *J Neurosci* 26:10253–10269. [CrossRef Medline](#)
- Iwasaki S, Chihara Y, Komuta Y, Ito K, Sahara Y (2008) Low-voltage-activated potassium channels underlie the regulation of intrinsic firing properties of rat vestibular ganglion cells. *J Neurophysiol* 100:2192–2204. [CrossRef](#)
- Iwasaki S, Nakajima T, Chihara Y, Inoue A, Fujimoto C, Yamasoba T (2012) Developmental changes in the expression of Kappav1 potassium channels in rat vestibular ganglion cells. *Brain Res* 1429:29–35. [CrossRef Medline](#)
- Johnston J, Forsythe ID, Kopp-Scheinpflug C (2010) Going native: voltage-gated potassium channels controlling neuronal excitability. *J Physiol* 588:3187–3200. [CrossRef Medline](#)
- Kalluri R, Xue J, Eatock RA (2010) Ion channels set spike timing regularity of mammalian vestibular afferent neurons. *J Neurophysiol* 104:2034–2051. [CrossRef Medline](#)
- Kanda Y (2013) Investigation of the freely available easy-to-use software 'EZR' for medical statistics. *Bone Marrow Transplant* 48:452–458. [CrossRef Medline](#)
- Karcz A, Hennig MH, Robbins CA, Tempel BL, Rübsamen R, Kopp-Scheinpflug C (2011) Low-voltage activated Kv1.1 subunits are crucial for the processing of sound source location in the lateral superior olive in mice. *J Physiol* 589:1143–1157. [CrossRef Medline](#)
- Karlsson J, von Hofsten J, Olsson PE (2001) Generating transparent zebrafish: a refined method to improve detection of gene expression during embryonic development. *Mar Biotechnol* 3:522–527. [CrossRef Medline](#)
- Kharkovets T, Hardelin JP, Safieddine S, Schweizer M, El-Amraoui A, Petit C, Jentsch TJ (2000) KCNQ4, a K⁺ channel mutated in a form of dominant deafness, is expressed in the inner ear and the central auditory pathway. *Proc Natl Acad Sci USA* 97:4333–4338. [Medline](#)
- Kharkovets T, Dedek K, Maier H, Schweizer M, Khimich D, Nouvian R, Vardanyan V, Leuwer R, Moser T, Jentsch TJ (2006) Mice with altered KCNQ4 K⁺ channels implicate sensory outer hair cells in human progressive deafness. *EMBO J* 25:642–652. [CrossRef Medline](#)

- Kohashi T, Oda Y (2008) Initiation of Mauthner- or non-Mauthner-mediated fast escape evoked by different modes of sensory input. *J Neurosci* 28:10641–10653. [CrossRef Medline](#)
- Kohashi T, Nakata N, Oda Y (2012) Effective sensory modality activating an escape triggering neuron switches during early development in zebrafish. *J Neurosci* 32:5810–5820. [CrossRef Medline](#)
- Kopp-Scheinpflug C, Fuchs K, Lippe WR, Tempel BL, Rübsamen R (2003) Decreased temporal precision of auditory signaling in Kcna1-null mice: an electrophysiological study in vivo. *J Neurosci* 23:9199–9207. [Medline](#)
- Lee RK, Eaton RC (1991) Identifiable reticulospinal neurons of the adult zebrafish, *Brachydanio rerio*. *J Comp Neur* 304:34–52. [CrossRef](#)
- Locke RE, Nerbonne JM (1997) Role of voltage-gated K⁺ currents in mediating the regular-spiking phenotype of callosal-projecting rat visual cortical neurons. *J Neurophysiol* 78:2321–2335. [Medline](#)
- Lysakowski A, Gaboyard-Niay S, Calin-Jageman I, Chatlani S, Price SD, Eatock RA (2011) Molecular microdomains in a sensory terminal, the vestibular calyx ending. *J Neurosci* 31:10101–10114. [CrossRef Medline](#)
- Maravall M, Stern EA, Svoboda K (2004) Development of intrinsic properties and excitability of layer 2/3 pyramidal neurons during a critical period for sensory maps in rat barrel cortex. *J Neurophysiol* 92:144–156. [CrossRef Medline](#)
- Marrs GS, Spirou GA (2012) Embryonic assembly of auditory circuits: spiral ganglion and brainstem. *J Physiol* 590:2391–2408. [CrossRef Medline](#)
- Metcalf WK, Mendelson B, Kimmel CB (1986) Segmental homologies among reticulospinal neurons in the hindbrain of the zebrafish larva. *J Comp Neur* 251:147–159. [CrossRef Medline](#)
- Nakajo K, Kubo Y (2005) Protein kinase C shifts the voltage dependence of KCNQ/M channels expressed in *Xenopus* oocytes. *J Physiol* 569:59–74. [CrossRef Medline](#)
- Nakamura Y, Takahashi T (2007) Developmental changes in potassium currents at the rat calyx of Held presynaptic terminal. *J Physiol* 581:1101–1112. [CrossRef Medline](#)
- Nakayama H, Oda Y (2004) Common sensory inputs and differential excitability of segmentally homologous reticulospinal neurons in the hindbrain. *J Neurosci* 24:3199–3209. [CrossRef Medline](#)
- Oertel D (1999) The role of timing in the brain stem auditory nuclei of vertebrates. *Annu Rev Physiol* 61:497–519. [CrossRef Medline](#)
- Patten SA, Sihra RK, Dhami KS, Coutts CA, Ali DW (2007) Differential expression of PKC isoforms in developing zebrafish. *Int J Dev Neurosci* 25:155–164. [CrossRef Medline](#)
- Pereda AE, Curti S, Hoge G, Cachope R, Flores CE, Rash JE (2013) Gap junction-mediated electrical transmission: regulatory mechanisms and plasticity. *Biochim Biophys Acta* 1828:134–146. [CrossRef](#)
- Pongs O, Schwarz JR (2010) Ancillary subunits associated with voltage-dependent K⁺ channels. *Physiol Rev* 90:755–796. [CrossRef Medline](#)
- Prescott SA, De Koninck Y (2002) Four cell types with distinctive membrane properties and morphologies in lamina I of the spinal dorsal horn of the adult rat. *J Physiol* 539:817–836. [Medline](#)
- Rasband MN, Park EW, Vanderah TW, Lai J, Porreca F, Trimmer JS (2001) Distinct potassium channels on pain-sensing neurons. *Proc Natl Acad Sci USA* 98:13373–13378. [CrossRef Medline](#)
- Reid MA, Flores-Otero J, Davis RL (2004) Firing patterns of type II spiral ganglion neurons in vitro. *J Neurosci* 24:733–742. [CrossRef Medline](#)
- Rhodes KJ, Monaghan MM, Barrezueta NX, Nawoschik S, Bekele-Arcuri Z, Matos MF, Nakahira K, Schechter LE, Trimmer JS (1996) Voltage-gated K⁺ channel beta subunits: expression and distribution of Kv beta 1 and Kv beta 2 in adult rat brain. *J Neurosci* 16:4846–4860. [Medline](#)
- Rocha-Sanchez SM, Morris KA, Kachar B, Nichols D, Fritzsche B, Beisel KW (2007) Developmental expression of Kcnq4 in vestibular neurons and neurosensory epithelia. *Brain Res* 1139:117–125. [CrossRef Medline](#)
- Rothman JS, Manis PB (2003a) Differential expression of three distinct potassium currents in the ventral cochlear nucleus. *J Neurophysiol* 89:3070–3082.
- Rothman JS, Manis PB (2003b) The roles potassium currents play in regulating the electrical activity of ventral cochlear nucleus neurons. *J Neurophysiol* 89:3097–3113.
- Smart SL, Lopantsev V, Zhang CL, Robbins CA, Wang H, Chiu SY, Schwartzkroin PA, Messing A, Tempel BL (1998) Deletion of the K(V)1.1 potassium channel causes epilepsy in mice. *Neuron* 20:809–819. [Medline](#)
- Soares D, Chitwood RA, Hyson RL, Carr CE (2002) Intrinsic neuronal properties of the chick nucleus angularis. *J Neurophysiol* 88:152–162. [Medline](#)
- Soh H, Pant R, LoTurco JJ, Tzingounis AV (2014) Conditional deletions of epilepsy-associated KCNQ2 and KCNQ3 channels from cerebral cortex cause differential effects on neuronal excitability. *J Neurosci* 34:5311–5321. [CrossRef Medline](#)
- Strutz-Seeböhm N, Seeböhm G, Fedorenko O, Baltaev R, Engel J, Knirsch M, Lang F (2006) Functional coassembly of KCNQ4 with KCNE-beta subunits in *Xenopus* oocytes. *Cell Physiol Biochem* 18:57–66. [CrossRef Medline](#)
- Szabo TM, McCormick CA, Faber DS (2007) Otolith endorgan input to the Mauthner neuron in the goldfish. *J Comp Neur* 505:511–525. [CrossRef Medline](#)
- Theiss RD, Kuo JJ, Heckman CJ (2007) Persistent inward currents in rat ventral horn neurones. *J Physiol* 580:507–522. [CrossRef Medline](#)
- Turrigiano G, Abbott LF, Marder E (1994) Activity-dependent changes in the intrinsic properties of cultured neurons. *Science* 264:974–977. [Medline](#)
- Turrigiano G, LeMasson G, Marder E (1995) Selective regulation of current densities underlies spontaneous changes in the activity of cultured neurons. *J Neurosci* 15:3640–3652. [Medline](#)
- Wang HS, McKinnon D (1995) Potassium currents in rat prevertebral and paravertebral sympathetic neurones: control of firing properties. *J Physiol* 485: 319–335. [CrossRef](#)
- Wang HS, Pan Z, Shi W, Brown BS, Wymore RS, Cohen IS, Dixon JE, McKinnon D (1998) KCNQ2 and KCNQ3 potassium channel subunits: molecular correlates of the M-channel. *Science* 282:1890–1893. [Medline](#)
- Watanabe T, Shimazaki T, Mishiho A, Suzuki T, Hirata H, Tanimoto M, Oda Y (2014) Coexpression of auxiliary Kvbeta2 subunits with Kv1.1 channels is required for developmental acquisition of unique firing properties of zebrafish Mauthner cells. *J Neurophysiol* 111: 1153–1164. [CrossRef](#)
- Wu C, Sharma K, Laster K, Hersi M, Torres C, Lukas TJ, Moore EJ (2014) Kcnq1-5 (Kv7.1-5) potassium channel expression in the adult zebrafish. *BMC Physiol* 14:1. [CrossRef Medline](#)
- Xu T, Nie L, Zhang Y, Mo J, Feng W, Wei D, Petrov E, Calisto LE, Kachar B, Beisel KW, Vazquez AE, Yamoah EN (2007) Roles of alternative splicing in the functional properties of inner ear-specific KCNQ4 channels. *J Biol Chem* 282:23899–23909. [CrossRef Medline](#)
- Zaika O, Lara LS, Gamper N, Hilgemann DW, Jaffe DB, Shapiro MS (2006) Angiotensin II regulates neuronal excitability via phosphatidylinositol 4,5-bisphosphate-dependent modulation of Kv7 (M-type) K⁺ channels. *J Physiol* 575:49–67. [CrossRef Medline](#)
- Zottoli SJ (1977) Correlation of the startle reflex and Mauthner cell auditory responses in unrestrained goldfish. *J Exp Biol* 66:243–254. [Medline](#)